

Precision Mass Measurements of $^{129-131}\text{Cd}$ and Their Impact on Stellar Nucleosynthesis via the Rapid Neutron Capture Process

D. Atanasov,¹ P. Ascher,¹ K. Blaum,¹ R. B. Cakirli,² T. E. Cocolios,³ S. George,¹ F. Herfurth,⁴
D. Kisler,¹ M. Kowalska,⁵ S. Kreim,^{1,5} Yu. A. Litvinov,⁴ D. Lunney,⁶ V. Manea,⁶ D. Neidherr,⁴
M. Rosenbusch,⁷ L. Schweikhard,⁷ A. Welker,⁸ F. Wienholtz,⁷ R. N. Wolf,¹ and K. Zuber⁸

¹*Max-Planck-Institut für Kernphysik, Saupfercheckweg 1, 69117 Heidelberg, Germany*

²*Department of Physics, University of Istanbul, 34134 Istanbul, Turkey*

³*University of Manchester, Manchester M13 9PL, United Kingdom*

⁴*GSI Helmholtzzentrum für Schwerionenforschung GmbH, 64291 Darmstadt, Germany*

⁵*CERN, 1211 Geneva, Switzerland*

⁶*CSNSM-IN2P3-CNRS, Université Paris-Sud, 91406 Orsay, France*

⁷*Ernst-Moritz-Arndt-Universität, Institut für Physik, 17487 Greifswald, Germany*

⁸*Technische Universität Dresden, 01069 Dresden, Germany*

(Dated: December 02, 2015)

Masses adjacent to the classical waiting-point nuclide ^{130}Cd have been measured by using the Penning-trap spectrometer ISOLTRAP at ISOLDE/CERN. We find a significant deviation of over 400 keV from earlier values evaluated by using nuclear beta-decay data. The new measurements show the reduction of the $N = 82$ shell gap below the doubly magic ^{132}Sn . The nucleosynthesis associated with the ejected wind from type-II supernovae as well as from compact object binary mergers is studied, by using state-of-the-art hydrodynamic simulations. We find a consistent and direct impact of the newly measured masses on the calculated abundances in the $A = 128 - 132$ region and a reduction of the uncertainties from the precision mass input data.

PACS numbers: 1.10.Dr, 07.75.+h, 26.30.Hj

The origin of the elements heavier than iron remains one of the major quests of today's observational, experimental, and theoretical physics. Produced by neutron capture reactions [1] various isotopes are created in radically different environments with time scales ranging from millions of years [2] for the slow (s) neutron capture process to seconds for the rapid (r) neutron capture process [3]. Imprints from the nuclear structure are found in the form of peaks on the solar abundance curve associated with the closed nuclear shells at neutron magic numbers $N = 50, 82$ and 126 . The description of these peaks in astrophysical simulations naturally has a strong sensitivity to the underlying nuclear structure as well as the fundamental choice of the yet-unknown associated astrophysical scenario.

Presently, the favored sites for the r process are core-collapse supernovae and the coalescence of two neutron stars (NS-NS) or a black hole and a neutron star (BH-NS) [3]. The heat associated with beta-decaying isotopes following an r process in the merger scenarios should lead to observable thermal emission, called a macro- or kilonova [4, 5]. The recent observation of an optical transient following a gamma-ray burst has been interpreted as such [6, 7]. This tantalizing evidence for an r -process site has triggered intense theoretical modeling. A comprehensive study was recently published [8] that addresses nucleosynthesis via the r process resulting from NS-NS and BH-NS mergers within a state-of-the-art hydrodynamic simulation.

However, nuclear data serving as crucial input for the astrophysical models are still lacking due to the difficulties in the production and measurement of the required

exotic isotopes. Indeed, many of the nuclides involved lie so far from stability that they may never be produced in the laboratory. In this case, nuclear theory is indispensable and many approaches have been proposed (see [9] for a review). Whether phenomenological or microscopic, mass models rely on measured masses for adjusting their parameters. While measuring masses farther from stability should help constrain the predictions, the final impact depends on how many new masses are used, how far they are from what is known, and the less quantifiable inherent uncertainty of the model. These points have been addressed in a recent study [10]. Despite regular progress of microscopic nuclear theory, such as Hartree-Fock-Bogoliubov models and density functional theory that provide complete and consistent data libraries, there are still significant deviations of predictions from experiment. Therefore, considerable efforts have been devoted to improve the production yields and selectivity of exotic nuclear species, as well as the sensitivity of experimental mass spectrometry.

In this Letter, we report the precision mass measurement of the closed shell nuclide ^{130}Cd , previously investigated by beta-gamma-decay spectroscopy [11], as well as the first mass determinations of its neighboring isotopes, allowing further examination of the strength of the $N = 82$ shell closure beyond the doubly magic ^{132}Sn . In addition to the inherent interest in doubly magic nuclides, the high abundances of isotopes around magic numbers make their associated nucleosynthesis sensitive to nuclear physics input, particularly the $A = 130$ region, as shown by systematic studies [12].

The new mass measurements were performed at the on-

line radioactive ion beam facility ISOLDE/CERN [13] using the ISOLTRAP mass spectrometer. The ISOLTRAP setup consists of a linear segmented radio-frequency quadrupole trap (RFQ), a multireflection time-of-flight mass separator (MR-TOF MS), a preparation, and a precision Penning trap, each of the latter two placed in the center of a superconducting magnet [14–16]. Depending on the half-life and production yield of the ion of interest, the mass determination is performed either by the time-of-flight ion-cyclotron resonance technique (TOF-ICR) using the precision Penning trap [17] or by performing the time-of-flight mass spectrometry with the MR-TOF MS [18].

Over the past three decades, TOF-ICR has proven to be the method of choice in the context of precision mass measurements of short-lived isotopes [19]. The method is based on the precise measurement of the cyclotron frequency $[\nu_c = qB/(2\pi m)]$ of an ion with mass m and charge q confined in a magnetic field with strength B . The calibration of B is performed before and after a measurement of the isotope of interest via the cyclotron frequency $\nu_{c,ref}$ of a reference isotope with a well-known mass. The frequency ratio $r = \nu_{c,ref}/\nu_c$ then yields directly the mass ratio and allows determining the mass of the ion of interest [20].

The MR-TOF MS recently implemented at ISOLTRAP [15, 21] relies on the determination of the ions' flight time (t) after multiple revolutions between two electrostatic mirrors. The time of flight of an ion with mass m is given by $t = \alpha(m/q)^{1/2} + \beta$, where the two parameters α and β are determined by the flight times $t_{1,2}$ of reference isotopes with well-known masses $m_{1,2}$, respectively. Substituting α and β in the previous formula leads to a more general relation for the mass of interest:

$$\sqrt{m} = C_{TOF}(\sqrt{m_1} - \sqrt{m_2}) + 0.5 * (\sqrt{m_1} + \sqrt{m_2}),$$

where $C_{TOF} = (2t - t_1 - t_2)/2(t_1 - t_2)$ is the experimental time-of-flight ratio [21].

The $^{129-131}\text{Cd}$ isotopes were produced by neutron-induced fission in a $50\text{g}/\text{cm}^2$ uranium-carbide target. The neutrons were created by a pulsed proton beam with an energy of 1.4 GeV impinging on a tungsten rod [22]. The resulting cadmium atoms diffused out of the heated target through a transfer line to an ion source. A quartz insert in the transfer line reduced the abundantly produced cesium and indium contamination [23]. Element-selective, stepwise resonant photoionization was performed by tunable laser radiation [24].

The cadmium ion beam was then transported towards ISOLTRAP at a kinetic energy of 30 keV through the two-stage high-resolution mass separator. The beam entering ISOLTRAP was accumulated in the RFQ, where it was bunched and cooled via collisions with helium buffer gas for 20 ms. The ion bunch was then extracted, and prior to injection in the MR-TOF MS its energy was adjusted by a pulsed drift cavity to the beam line potential. Ions were then captured in the MR-TOF MS by use of

the in-trap lift technique [25]. After a trapping time for sufficient separation between the ions of interest and the remaining contaminants, the ions were transported either to the Penning traps or to an ion detector.

For the cases of $^{129-131}\text{Cd}^+$, the MR-TOF MS was employed to provide purified samples for the Penning traps with trapping times of 1.37 and 13.71 ms, respectively. In the preparation Penning trap, the ions were cooled and recentered for 80 ms in a helium buffer-gas environment. Afterwards, the ion bunch was transported to the precision Penning trap for the TOF-ICR measurement with a Ramsey-type excitation [26]. The excitation timing patterns $\tau_{rf}^{on} - \tau_{rf}^{off} - \tau_{rf}^{on}$ used in this experiment were 20-160-20 ms (for $A = 129$) and 10-80-10 ms (for $A = 130$). An example of a TOF-ICR resonance curve is presented in the upper panel of Fig. 1. It shows the ions' mean time of flight as a function of the frequency of the quadrupolar excitation, where the center frequency corresponds to the cyclotron frequency ν_c of $^{130}\text{Cd}^+$. In summary, four TOF-ICR measurements of ^{129}Cd were performed, as well as three of ^{130}Cd , totaling more than 1500 and 550 events, respectively.

Considering the low efficiency and the short half-life of $^{131}\text{Cd}^+$, the mass measurements were performed by using the faster MR-TOF MS technique. The calibration of the device was performed by using off-line reference ions of stable $^{133}\text{Cd}^+$, as well as the on-line radioactive ions of surface-ionized $^{131}\text{Cd}^+$ delivered with $^{131}\text{Cd}^+$

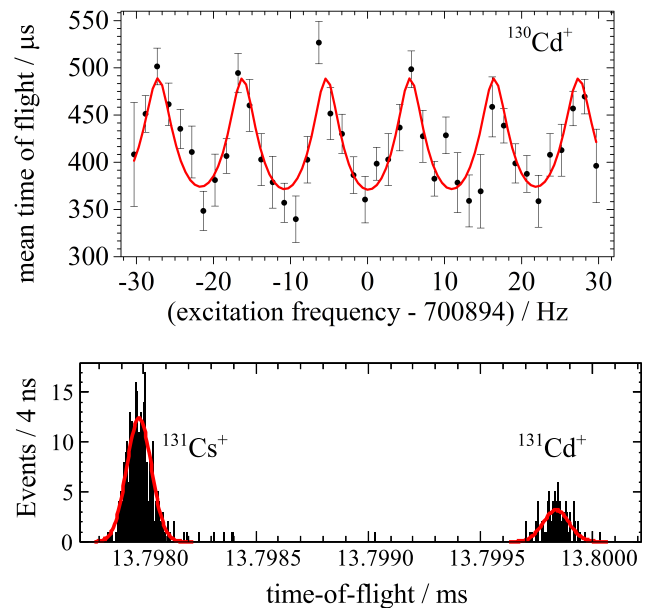


Figure 1: (Color online) *Upper panel*: A typical spectrum showing the TOF-ICR resonance of $^{130}\text{Cd}^+$ ions using a Ramsey-type excitation scheme [26]. The line represents a fit to the data points where the center frequency corresponds to the cyclotron frequency. *Lower panel*: MR-TOF mass spectrum, i.e. Number of events as a function of the flight times of $^{131}\text{Cs}^+$ and $^{131}\text{Cd}^+$.

Table I: Frequency ratios ($r = \nu_{c,ref}/\nu_c$), time-of-flight ratio (C_{ToF}), mass excess (ME) and the neutron separation energy (S_n) of the cadmium isotopes measured in this work. Values of the mass excess from the Atomic Mass Evaluation 2012 (AME12) [27] are given as well (# indicates extrapolated values). The masses of the references ions used in the evaluation are $m(^{131}\text{Cs}) = 130905465(5)\mu\text{u}$ and $m(^{133}\text{Cs}) = 132905451.961(9)\mu\text{u}$ (from AME12). Experimental half-lives are taken from [28–30]. The yield values are only estimates, given the imprecise knowledge of the ISOLTRAP efficiency.

| A | Yield (Ions/ μC) | Half-life (ms) | Reference | Ratio r or C_{ToF} | Mass Excess (keV) | | S_n (MeV) |
|-----|------------------------------|-----------------------------|-----------------------|----------------------------|--------------------------|----------------|-------------|
| | | | | | New | AME12 | |
| 129 | 1200 | 151(15),146(8) ^a | ¹³³ Cs | $r = 0.970105338(136)$ | -63 148(74) ^b | -63 510#(200#) | 3.977(74) |
| 130 | >1000 | 127(2) | ¹³³ Cs | $r = 0.977645186(180)$ | -61 118(22) | -61 530(160) | 6.131(29) |
| 131 | >100 | 98.0(2) | ^{131,133} Cs | $C_{ToF} = 0.4823044(539)$ | -55 215(100) | -55 331#(196#) | 2.169(103) |

^aThe values correspond to $11/2^-$ and $3/2^+$ states, respectively.

^bThe mass excess shown in the table is an estimate of the ground-state value based on the measured value of -63 058(17) keV (from the frequency ratio) and the allowance of a ground-state and isomer mixture (see the text for details).

[18, 31]. In total, 11 spectra were recorded at different numbers of revolutions 500, 800, and 1000, corresponding to MR-TOF trapping times of 13.77, 22.02, and 27.51 ms, respectively, and totaling more than 1350 events. An example of the obtained spectra is shown in the lower panel of Fig. 1; the fit method assumes a Gaussian distribution. Our results are in agreement within statistical uncertainties with the method using a hybrid Gaussian distribution [32] for the peak fits. The final frequency and time-of-flight ratios are listed in Table I.

The beam of ¹²⁹Cd⁺ likely contained two nuclear states, previously identified and measured at ISOLDE. The spins of the two states were assigned to $11/2$ and $3/2$ by hyperfine structure measurements [33]. The estimated energy difference between the ground and the isomeric state was inferred from systematics in the cadmium chain to be about 180(100) keV [34]. As a definite assignment of the determined ¹²⁹Cd⁺ frequency ratio to one of the two nuclear states is not possible, an estimation for the pure ground-state mass excess can be determined according to Appendix B of Ref. [27], resulting in $ME = -63\,148(74)$ keV. The neutron-separation energies (S_n) around the magic neutron number $N = 82$ presented in Table I were computed by using the newly determined masses. The drop of S_n at the crossing of neutron magic numbers is one of the important signatures for nuclear magicity, associated with large gaps in the spectra of single-particle energies obtained from shell-model or mean-field approaches.

In agreement with the indications of the earlier beta decay results, our precision mass measurements strengthen and quantify the decrease of the shell strength below ¹³²Sn. Specifically, we observe a reduction of the empirical one-neutron shell gap by 1 MeV between ¹³²Sn ($Z = 50$) and ¹³⁰Cd ($Z = 48$), also highlighting the doubly magic character of ¹³²Sn.

In Fig. 2, the experimental values of the empirical shell gap, defined as $S_n(N = 82) - S_n(N = 83)$, are pre-

sented. Shown in the figure as well are the predictions of two different mass models, commonly employed to provide input mass data for various r -process calculations. We note that the microscopic HFB-24 model [36] predicts a significant reduction of the empirical shell gap for $Z < 50$, while the microscopic-macroscopic finite-range droplet model [35] predicts a rather constant shell gap, despite the very close absolute value.

The ¹³⁰Cd s expected to be the progenitor feeding through β decay the second large abundance peak at $A \approx 130$ in the Solar System abundance, corresponding to a region around the stable ¹³⁰Te. The impact of mass predictions on the r -process nucleosynthesis in general remains difficult to ascertain, in the sense that their

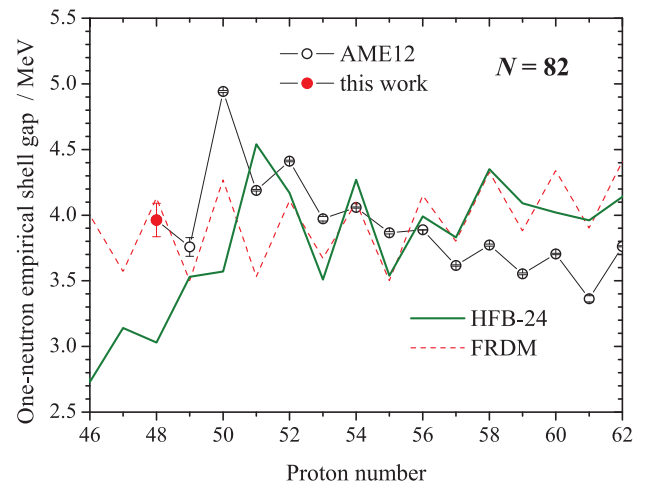


Figure 2: (Color online). The empirical one-neutron shell gap. The black open circles use the available data from the Atomic Mass Evaluation [27] and the red filled circle is the ¹³⁰Cd value calculated using the masses from this work. Theoretical values from two mass models are presented for comparison, the finite-range droplet model (FRDM) [35] and HFB-24 [36].

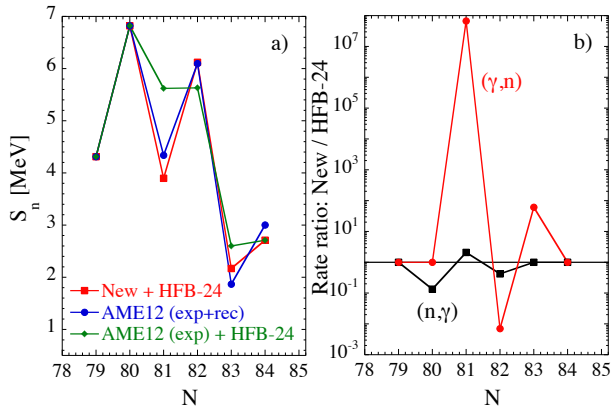


Figure 3: (a) Neutron-separation energies (S_n) as a function of neutron number for the newly measured masses (red) in comparison to data in this region from AME12, complemented with extrapolated (recommended) values (blue) or with HFB-24 calculations (green) [36]. (b) Ratio of the neutron capture (n,γ) and photo-disintegration (γ,n) rates obtained with experimental masses from this work and the HFB-24 model.

influence strongly depends on the adopted astrophysical scenario and most particularly on the temperature at which the r process takes place [37]. In the so-called cold r process, photodisintegration rates are slow, and consequently no $(n,\gamma) - (\gamma,n)$ equilibrium can be achieved. Here nuclear masses influence the calculated abundances not only through the competition between the two inverse (n,γ) and (γ,n) processes, but also through the neutron capture competition with the β decay [3].

In the present application, the newly measured masses are used to estimate the neutron capture and photodisintegration rates but not the β -decay half-lives (experimental half-lives being available in this mass region [28, 34]). The reaction rates are calculated by using the TALYS reaction code [38, 39]. The impact of the new masses on the reaction rates is illustrated in Fig. 3 (right panel), where the Maxwellian-averaged radiative neutron capture and the photoneutron emission rates at $T = 10^9$ K are compared when considering a set of nuclear masses from the AME12, complemented with the masses measured in this work, or calculations from the HFB-24 model. Since the neutron-separation energies are affected, the ratio of the neutron capture to the photoneutron rates is also affected by the new measurements, so that, even if a $(n,\gamma) - (\gamma,n)$ equilibrium is established within the Cd isotopic chain, the relative isotopic abundances may be affected.

Despite a growing wealth of observational data (see, e.g., Refs. [40, 41]) and increasingly better r -process models with new astrophysical or nuclear physics ingredients, the stellar production site(s) of r -process material has (have) not been identified yet (for a review, see [3]). All proposed scenarios face serious problems. For illustrative purposes, we consider two widely discussed r -process

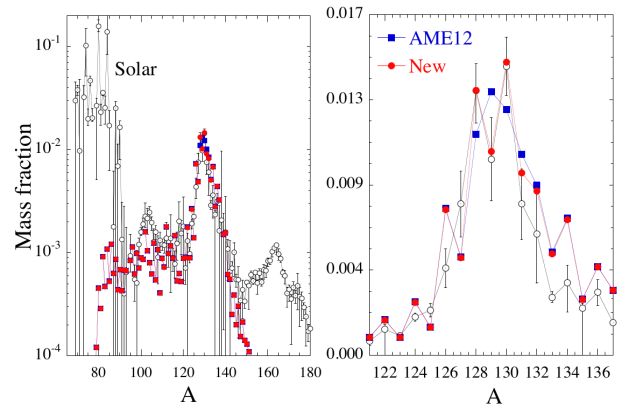


Figure 4: (Color online) Calculated distributions of the r -process abundance pattern obtained within the ν -driven wind scenario, see text for conditions and [3, 43] for more details. The blue squares are obtained from AME12 (complemented with HFB-24 masses for experimentally unknown isotopes) and corresponding rates, while the red circles include the new Cd masses. For comparison, the r -process solar abundance distribution is shown by open circles. Both theoretical distributions are normalized by the same factor, such that the mass fraction of ^{128}Te obtained with the new Cd masses reproduces the solar value.

models, namely, the ν -driven wind model in core-collapse super-nova explosions of massive stars [42–44] and the decompression of NS matter during NS-NS and NS-BH mergers, including the neutrino and viscously driven outflows generated during the postmerger remnant evolution of the relic BH-torus system [8, 45, 46]. Details concerning the postprocessing of the simulations can be found in Refs. [45, 47].

In the ν -driven wind scenario, the adopted wind model corresponds to a subsonic breeze expansion with an entropy $s_{kB} = 193$, electron fraction $Y_e = 0.48$, mass loss rate $dM/dt = 6 \times 10^{-7} M_\odot \text{ s}^{-1}$ and breeze solution $f_w = 3$ (see [3, 43] for more details). For such conditions, the $A \simeq 130$ nuclei are dominantly produced and the expansion is rather fast, so that the neutron irradiation responsible for the r processing takes place at a rather low temperature and the final abundance distribution is sensitive to the adopted neutron capture rates. This specific event is chosen since it is found to strongly produce isotopes around the second r -process peak, as shown in Fig. 4. The modified rates based on the new Cd masses are seen to have an impact in the $A \simeq 130$ region. In particular, the odd-even effect between $A = 128$ and $A = 130$ is significantly modified due to the changes in the neutron-separation energies, especially for ^{129}Cd (Fig. 3). This first example shows that the three newly measured masses affect directly the r -process abundance distribution in this specific ν -driven wind scenario, which could potentially explain the origin of the Solar System of r nuclei in the vicinity of the second $A \simeq 130$ peak despite all the remaining uncertainties still affecting the

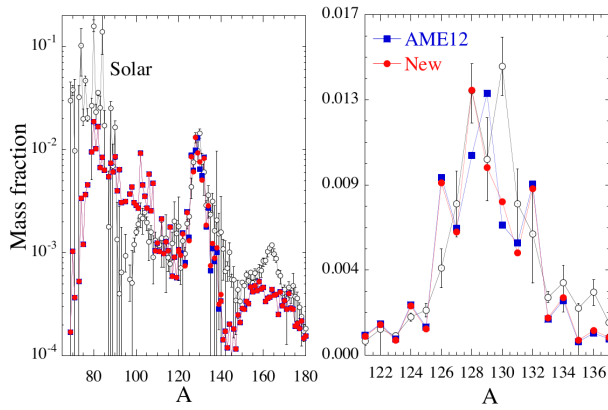


Figure 5: (Color online) Same as Fig. 4 but showing the final r -process abundance curve for viscously driven ejecta from a $3 M_{\odot}$ BH - $0.1 M_{\odot}$ torus system model.

astrophysical modeling of this site. For the compact binary merger scenario, we do not study the nucleosynthesis in the matter that is dynamically ejected by tidal and pressure forces during the merging of the two compact objects but rather in the neutrino and viscously driven outflows generated during the postmerger remnant evolution of the relic BH-torus systems. Indeed, in the prompt ejecta, large neutron-to-seed ratios drive the nuclear flow into the very heavy-mass region along a path close to the neutron drip line, leading to multiple fission recycling at relatively low temperatures, and essentially $A > 140$ nuclei are found to be produced. In contrast, the BH-torus ejecta produce heavy elements in the range from $A \sim 80$ up to thorium and uranium with a significant contribution to the $A \simeq 130$ abundance peak. We consider here a representative sample of 310 trajectories ejected from a system characterized by a torus mass of $0.1 M_{\text{dot}}$ and a $3 M_{\text{dot}}$ BH (corresponding to the M3A8m1a5 model of Ref. [8]). The total mass ejected from the BH-torus system amounts to $2.5 \times 10^{-2} M_{\odot}$, and the outflow is characterized by a mean electron fraction $\bar{Y}_e = 0.24$, a mean entropy $\bar{s}/k_B = 28$, and a mean velocity $\bar{v} = 1.56 \times 10^9$ cm/s.

The impact of the newly measured masses is shown in Fig. 5 and seen to give rise to an abundance peak that is now shifted by one unit; i.e., the peak location is now at

$A = 128$ and $A = 129$. Interestingly, despite the fact that the present distribution results from a mass-weighted average of hundreds of trajectories, the modification of only three masses still has an impact on the abundance ratio in the corresponding region. This property is linked to the fact that the masses affect directly the top of the $A = 130$ peak.

In conclusion, the masses of $^{129-131}\text{Cd}$ were determined with high precision using the Penning-trap mass spectrometer ISOLTRAP. The new masses show a significant reduction of the $N = 82$ shell gap for $Z < 50$. The new data provide additional constraints for nuclear theory, considering the diverging predictions of mass models concerning the $N = 82$ empirical shell gap for $Z < 50$. Clearly, the new measurements bring reliability to the description of r -process nucleosynthesis by reducing the uncertainty from the nuclear-physics input. Given the large volume of data required for r -process calculations, it is remarkable that only three masses make an observable impact on the predicted abundances, highlighting the importance of precision measurements in this region of the nuclear chart.

Acknowledgments

The authors thank G. Audi, CSNSM-IN2P3-CNRS, for the fruitful discussion in the process of data analysis. We thank the ISOLDE technical group and the ISOLDE Collaboration for their support. We acknowledge support by the BMBF (05P12HGC11, 05P12HGFNE, 05P15HGCIA, and 05P09ODCIA), Nuclear Astrophysics Virtual Institute (NAVI) of the Helmholtz Association, Helmholtz-CAS Joint Research Group (HCJRG-108), the Max-Planck Society, the European Union 7th framework through ENSAR (Contract No. 262010), the French IN2P3, the Helmholtz Alliance Program, Contract No. HA216/EMMI, by the STFC under Grants No. ST/L005743/1 and No. ST/L005816/1. D. A. acknowledges support by the IMPRS-PTFS. S. Goriely acknowledges financial support from FRS-FNRS (Belgium). O. J. acknowledges support from Max-Planck/Princeton Center for Plasma Physics (MPPC). S. K. acknowledges support from the Robert- Bosch Foundation. R. B. C. acknowledges support by the Max-Planck Partner group.

-
- [1] E. M. Burbidge, G. R. Burbidge, W. A. Fowler, and F. Hoyle, *Rev. Mod. Phys.* **29**, 547 (1957).
 - [2] P. Neyskens et al., *Nature* **517**, 174 (2015).
 - [3] M. Arnould et al., *Phys. Rep.* **450**, 97 (2007).
 - [4] L.-X. Li and B. Paczyński, *Astrophys. J.* **507**, L59 (1998).
 - [5] S. R. Kulkarni, arXiv **astro-ph**, 0510256 (2005).
 - [6] N. R. Tanvir et al., *Nature* **500**, 547 (2013).
 - [7] E. Berger, W. Fong, and R. Chornock, *Astrophys. J. Lett.* **774**, L23 (2013).
 - [8] O. Just et al., *Month. Not. Roy. Astron. Soc.* **448**, 541 (2015).
 - [9] D. Lunney, J. M. Pearson, and C. Thibault, *Rev. Mod. Phys.* **75**, 1021 (2003).
 - [10] J. D. McDonnell et al., *Phys. Rev. Lett.* **114**, 122501 (2015).
 - [11] I. Dillmann et al., *Phys. Rev. Lett.* **91**, 162503 (2003).
 - [12] M. Mumpower et al., *J. Phys. G* **42**, 034027 (2015).
 - [13] E. Kugler, *Hyp. Int.* **129**, 23 (2000).

- [14] M. Mukherjee et al., *Eur. Phys. J. A* **35**, 1 (2008).
- [15] R. Wolf et al., *Nucl. Instrum. & Methods A* **686**, 82 (2012).
- [16] S. Kreim et al., *Nucl. Instrum. & Methods B* **317**, 492 (2013).
- [17] K. Blaum, *Phys. Rep.* **425**, 1 (2006).
- [18] F. Wienholtz et al., *Nature* **498**, 346 (2013).
- [19] K. Blaum, J. Dilling, and W. Nörtershäuser, *Phys. Scr.* **2013**, 014017 (2013).
- [20] M. König et al., *Int. J. Mass Spectrom.* **142**, 95 (1995).
- [21] R. Wolf et al., *Int. J. Mass Spectrom.* **349-350**, 123 (2013), 100 years of Mass Spectrometry.
- [22] U. Köster, *Eur. Phys. J. A* **15**, 255 (2002).
- [23] E. Bouquerel et al., *Eur. Phys. J Special Topics* **150**, 277 (2007).
- [24] B. A. Marsh, *Rev. Sci. Instrum.* **85** (2014).
- [25] R. N. Wolf et al., *Int. J. Mass Spectrom.* **313**, 8 (2012).
- [26] S. George et al., *Int. J. Mass Spectrom.* **264**, 110 (2007).
- [27] G. Audi et al., *Chinese Phys. C* **36**, 1287 (2012).
- [28] G. Lorusso et al., *Phys. Rev. Lett.* **114**, 192501 (2015).
- [29] J. Taprogge et al., *Phys. Rev. C* **91**, 054324 (2015).
- [30] K. Kratz et al., *Eur. Phys. J. A* **25**, 633 (2005).
- [31] M. Rosenbusch et al., *Phys. Rev. Lett.* **114**, 202501 (2015).
- [32] P. Schury et al., *Nucl. Instrum. & Methods B* **335**, 39 (2014).
- [33] D. T. Yordanov et al., *Phys. Rev. Lett.* **110**, 192501 (2013).
- [34] G. Audi et al., *Chinese Phys. C* **36**, 1157 (2012).
- [35] P. Moller, J. Nix, W. Myers, and W. Swiatecki, *At. Data Nucl. Data Tables* **59**, 185 (1995).
- [36] S. Goriely, N. Chamel, and J. M. Pearson, *Phys. Rev. C* **88**, 024308 (2013).
- [37] A. Arcones and G. Martínez-Pinedo, *Phys. Rev. C* **83**, 045809 (2011).
- [38] A. J. Koning, S. Hilaire, and M. C. Duijvestijn, *Nucl. Data Science and Technology* pp. 211–214 (2008), (EDP Sciences; eds O. Bersillon et al.).
- [39] S. Goriely, S. Hilaire, and A. J. Koning, *Astron. Astrophys.* **487**, 767 (2008).
- [40] C. Sneden, J. J. Cowan, and R. Gallino, *Annu. Rev. Astron. Astrophys.* **46**, 241 (2008).
- [41] I. U. Roederer, *Astrophys. J. Lett.* **732**, L17 (2011).
- [42] K. Takahashi, J. Wittig, and H. Janka, *Astron. Astrophys.* **286**, 857 (1994).
- [43] K. Takahashi and H. Janka, Singapore: World Scientific **213** (1997).
- [44] S. Wanajo, H. Janka, and B. Müller, *Astrophys. J. Lett.* **726**, L15 (2011).
- [45] S. Goriely, A. Bauswein, and H. Janka, *Astrophys. J. Lett.* **738**, L32 (2011).
- [46] A. Bauswein, S. Goriely, and H. Janka, *Astrophys. J.* **773**, 78 (2013).
- [47] S. Goriely et al., *Phys. Rev. Lett.* **111**, 242502 (2013).